

Synthesis of thermally stable HfO_xN_y as gate dielectric for AlGaN/GaN heterostructure field-effect transistors

Tong Zhang(张彤), Taofei Pu(蒲涛飞), Tian Xie(谢天), Liuan Li(李柳暗), Yuyu Bu(补钰煜), Xiao Wang(王霄), Jin-Ping Ao(敖金平)

Citation: Chin. Phys. B . 2018, 27(7): 078503. **doi:** 10.1088/1674-1056/27/7/078503

Journal homepage: http://cpb.iphy.ac.cn; http://iopscience.iop.org/cpb

What follows is a list of articles you may be interested in

Scalability of dark current in silicon PIN photodiode

Ya-Jie Feng(丰亚洁), Chong Li(李冲), Qiao-Li Liu(刘巧莉), Hua-Qiang Wang(王华强), An-Qi Hu(胡安琪), Xiao-Ying He(何晓颖), Xia Guo(郭霞)

Chin. Phys. B . 2018, 27(4): 048501. **doi:** 10.1088/1674-1056/27/4/048501

Enhanced radiation-induced narrow channel effects in 0.13-μm PDSOI nMOSFETs with shallow trench isolation

Meng-Ying Zhang(张梦映), Zhi-Yuan Hu(胡志远), Da-Wei Bi(毕大炜), Li-Hua Dai(戴丽华), Zheng-Xuan Zhang(张正选)

Chin. Phys. B . 2018, 27(2): 028501. **doi:** 10.1088/1674-1056/27/2/028501

Equivalent oxide thickness scaling of Al_2O_3/Ge metal-oxide-semiconductor capacitors with ozone post oxidation

Sun Jia-Bao, Yang Zhou-Wei, Geng Yang, Lu Hong-Liang, Wu Wang-Ran, Ye Xiang-Dong, David Zhang Wei, Shi Yi, Zhao Yi

Chin. Phys. B . 2013, 22(6): 067701. **doi:** 10.1088/1674-1056/22/6/067701

Evidence of GeO volatilization and its effect on the characteristics of HfO_2 grown on Ge substrate

Fan Ji-Bin, Liu Hong-Xia, Fei Cheng-Xi, Ma Fei, Fan Xiao-Jiao, Hao Yue

Chin. Phys. B . 2013, 22(3): 037702. **doi:** 10.1088/1674-1056/22/3/037702

Analytical model including the fringing-induced barrier lowering effect for a dual-material surrounding-gate MOSFET with a high-κ gate dielectric

Li Cong,Zhuang Yi-Qi,Zhang Li,Bao Jun-Lin

Chin. Phys. B . 2012, 21(4): 048501. **doi:** 10.1088/1674-1056/21/4/048501

Synthesis of thermally stable HfO_xN_y as gate dielectric for AlGaN/GaN heterostructure field-effect transistors*

Tong Zhang(张彤)[1], Taofei Pu(蒲涛飞)[1], Tian Xie(谢天)[1], Liuan Li(李柳暗)[2,†], Yuyu Bu(补钰煜)[3], Xiao Wang(王霄)[3], and Jin-Ping Ao(敖金平)[1,3,‡]

[1] *Institute of Technology and Science, Tokushima University, Tokushima* 770-8506, *Japan*
[2] *School of Electronics and Information Technology, Sun Yat-Sen University, Guangzhou* 510275, *China*
[3] *School of Microelectronics, Xidian University, Xi'an* 710071, *China*

(Received 25 January 2018; revised manuscript received 8 May 2018; published online 25 June 2018)

In this paper, we adopted thermally stable HfO_xN_y as gate dielectric for TiN/HfO_xN_y/AlGaN/GaN heterostructure field-effect transistors (HFETs) application. It demonstrated that the surface morphologies, composition, and optical properties of the HfO_xN_y films were dependent on oxygen flow rate in the O_2/N_2/Ar mixture sputtering ambient. The obtained metal–oxide–semiconductor heterostructure field-effect transistors by depositing HfO_2 and HfO_xN_y dielectric at different oxygen flow rates possessed a small hysteresis and a low leakage current. After post deposition annealing at 900 °C, the device using HfO_xN_y dielectric operated normally with good pinch-off characteristics, while obvious degradation are observed for the HfO_2 gated one at 600 °C. This result shows that the HfO_xN_y dielectric is a promising candidate for the self-aligned gate process.

Keywords: AlGaN/GaN HFET, gate dielectric, HfO_xN_y, thermal stability

PACS: 85.30.–z, 77.55.D–, 61.82.Ms, 68.60.Dv **DOI:** 10.1088/1674-1056/27/7/078503

1. Introduction

AlGaN/GaN heterostructure field-effect transistors (HFETs) have attracted many attentions for power and microwave applications due to the high mobility of the two-dimensional electron gas (2DEG).[1,2] To achieve high-gain millimeter-wave power amplification, a key challenge is to increase the maximum cut-off frequency (f_T). Self-aligned gate (SAG) structure is an effective method to minimize the access region (access resistance) of AlGaN/GaN HFETs, which is beneficial for achieving higher f_T.[3] In a SAG structure, the Schottky gate serves as mask for ohmic electrode deposition and anneals simultaneously with ohmic electrodes. The widely used Ti/Al-based multilayers on AlGaN/GaN HFETs need a high annealing temperature (commonly above 700 °C) to form ohmic contact, which usually causes a high gate leakage current of the Schottky contact and degrades the noise handling capacity.[4] One of the solutions is to develop a low temperature ohmic process (below 600 °C) with the assistance of inductivity coupled plasma (ICP) treatment, but it is difficult to control the etching depth and uniformity.[5,6] On the other hand, metal–oxide–semiconductor (MOS) HFETs with gate dielectric are helpful to decrease the gate leakage current. To meet the SAG process requirement, the dielectric should withstand the high annealing temperature. Besides, to scale down the gate length as well as the dielectric thickness for higher frequency, we usually adopt high dielectric constant (high-k) gate dielectric to suppress the serve leakage current.[7–9]

Among the various gate dielectrics, hafnium oxide (HfO_2) possesses high-k, wide bandgap, and acceptable band offsets with GaN ($\Delta E_C = 2.0$ eV and $\Delta E_V = 0.3$ eV), has been extensively investigated as a promising candidate.[10–12] However, the crystallization temperature of the HfO_2 film is usually close to 500 °C, which means that the microcrystalline structure appears after ohmic annealing at high temperature.[13] Then oxygen or dopants from the environment can easily diffuse into the gate dielectric via grain boundaries, leading to the increasing leakage current, threshold voltage (V_{th}) instability, and long-term dielectric reliability degradation.[14]

Recently, many studies focused on the hafnium oxynitride film (HfO_xN_y) by incorporating nitrogen into HfO_2. The existence of Hf–N bond in the bulk and N at the dielectric/GaN interface could act as a crystallization inhibitor, distort the equilibrium of the lattice, produce disordered states, and improve the thermal stability (crystallization temperatures up to 800–950 °C).[15–17] Because oxygen exhibits a stronger reactivity to Hf than nitrogen, we should control the oxygen flow rate to guarantee the excellent properties of HfO_xN_y dielectric.[18] Therefore, it is worthwhile to further study electrical and material characterizations of HfO_xN_y film. Herein, we tried to obtain HfO_xN_y film by optimizing the oxygen percentage in the N_2/Ar mixture sputtering ambient. Then we also explored the thermal stability of the TiN/HfO_xN_y gate stack structure.

*Project supported by the National Key Research and Development Program of China (Grant No. 2017YFB0403000).
†Corresponding author. E-mail: liliuan@mail.sysu.edu.cn
‡Corresponding author. E-mail: jpao@ee.tokushima-u.ac.jp
© 2018 Chinese Physical Society and IOP Publishing Ltd

2. Device fabrication

The epitaxial wafers used in this experiment are AlGaN/GaN HFETs grown on sapphire substrates by metal organic chemical vapor deposition. The device fabrication process started from ICP isolation with an etching depth of 100 nm. Ti/Al/Ti/Au (50/200/40/40 nm) multi-layers were used to form ohmic contact by annealing at 850 °C for 3 min in N_2. After gate pattern lithography, samples were immersed in diluted HCl (HCl:H_2O = 1 : 1) for over 5 min to remove the native oxide layer. A HfO_xN_y layer with a nominal thickness of 50 nm was deposited using reactive sputtering in a N_2, O_2, and Ar mixture ambient environment (Hf target with Ar : N : O = 15 : 15 :x, x = 0, 1, 3, and 5 sccm). A relatively smaller oxygen flow rate was selected because of the hafnium metal is easy to be oxidized. To investigate the thermal stability, the HfO_xN_y layer was annealed in N_2 ambient at 400, 600, 800, 900, and 1000 °C for 1 min, respectively. The TiN gate electrode (about 50 nm) with a cap layer of Ti/Au (10/40 nm) was formed by DC magnetron reactive sputtering, as shown in Fig. 1. Finally, post-deposition anneal was conducted in a N_2 ambient at 300 °C for 10 min to improve the contact.

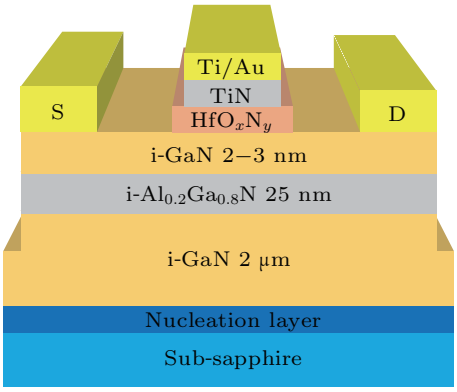


Fig. 1. (color online) The schematic structure of AlGaN/GaN MOS HFETs using HfO_xN_y gate dielectric.

3. Results and discussion

First, HfO_xN_y films are deposited on sapphire substrates to evaluate the effect of oxygen flow rate on the structure and properties. The surface morphologies and the growth rates of HfO_xN_y films are characterized using atomic force microscope. When introducing a low flow rate of oxygen (0 and 1 sccm), the surface of the samples consist with high density and small size particle (Figs. 2(a) and 2(b)). The root mean square roughnesses (RMSs) of those samples are approximately 0.12 and 0.13 nm, respectively. The particle size increased obviously for the sample deposited with a medium oxygen (3 sccm) (Fig. 2(c)), but the surface is still flat with a RMS of approximately 0.12 nm. Finally, the film obtained with 5 sccm oxygen showed the most rough morphology with a RMS of approximately 0.29 nm. Besides, obvious pits appeared on the surface, implying that the growth mode changed seriously. We calculated the average sputtering rates from dividing the total film thickness by the deposition times. The rates are approximately 0.83, 0.66, 0.56, and 0.42 nm/min with the oxygen flow rate of 0, 1, 3, and 5 sccm, respectively. When introducing oxygen into the chamber, the decrease of sputtering yield as well as the oxidation of the Hf target surface causes the decrease of sputtering rate. At a relatively low oxygen flow rate, the oxidation of the Hf target is very weak. The sputtered Hf atoms on the substrate surface have enough time to diffuse and react under a lower sputtering rate, resulting in a better surface roughness. While at a relatively high oxygen flow rate, the oxidization of metal target surface is much easier by oxygen because of the high bonding energy between oxygen and hafnium. Therefore, the sputtered HfO_2 on the substrate is relatively difficult to diffuse, which will deteriorate the film quality and cause the pit defect.

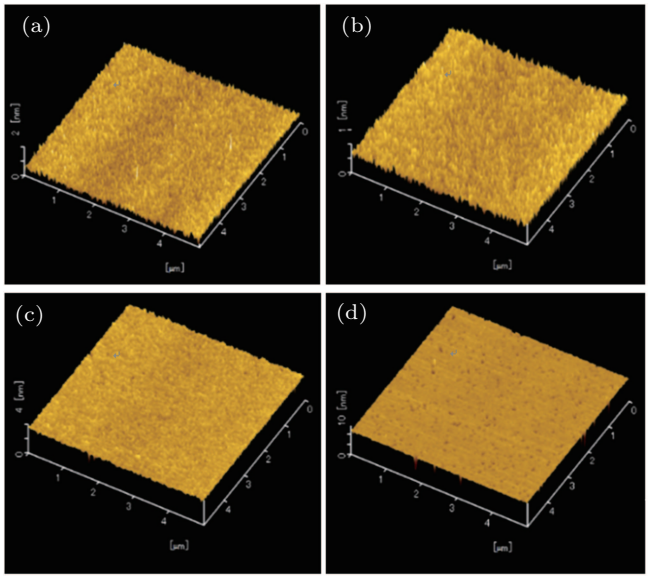


Fig. 2. (color online) The 5 μm×5 μm scaled surface morphology of the as-grown films with O_2 flow rate of (a) 0 sccm, (b) 1 sccm, (c) 3 sccm, and (d) 5 sccm.

The bonding status of the HfO_xN_y films were evaluated by x-ray photoelectron spectroscopy (XPS).[19–21] The Hf4f core level (CL) spectrum of the sample deposited without oxygen is dominated by two peaks at 14.4 eV and 16.0 eV, which agrees well with the reported values for HfN (Fig. 3(a)). The weak peak at around 17.5 eV may result from the surface oxidation due to the air exposure. Furthermore, the N–Hf peak at 396.7 eV in N1 s CL spectrum (Fig. 4(a)) and no detectable peak in O1 s CL spectrum (Fig. 5(a)) also confirm the above result. While for the sample deposited with 1 sccm oxygen, the Hf4f CL spectrum (Fig. 3(b)) has three obvious peaks at 16.2 eV, 17.1 eV, and 18.6 eV. The corresponding O1 s spectrum (Fig. 5(b)) shows two peaks at the binding energy of 530.5 and 531.1 eV. The peaks at 16.2 eV and 531.1 eV as well as the weak peak at 396.0 eV in N1 s CL spectrum (Fig. 4(b))

are assigned to the HfO_xN_y phase. Besides, the two peaks at 17.1 eV and 18.6 eV originate from Hf bounded to oxygen. This also can be confirmed from the Hf4f CL spectrum of the sample deposited with 5 sccm oxygen, in which two peaks at 17.2 eV and 18.9 eV dominate the spectrum (Fig. 3(c)). Furthermore, an enhanced peak at 530.5 eV dominating the O1 s CL spectrum (Fig. 5(c)) as well as weak peak in N1 s CL spectrum (Fig. 4(c)) indicates that HfO_2 becomes the dominate phase with 5 sccm oxygen because of the higher bonding energy between oxygen and hafnium.

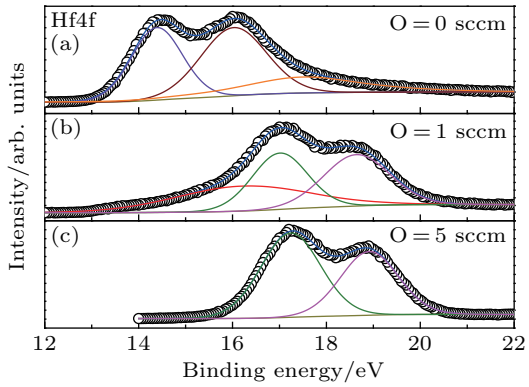


Fig. 3. (color online) The fitted Hf4f spectra for the samples obtained with different oxygen flow rates.

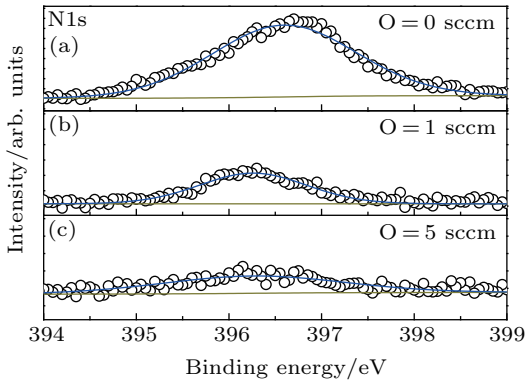


Fig. 4. (color online) The fitted N1s spectra for the samples obtained with different oxygen flow rates.

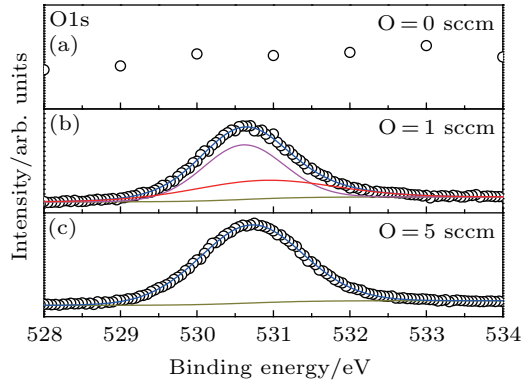


Fig. 5. (color online) The fitted O1s spectra for the samples obtained with different oxygen flow rates.

UV–vis diffuse reflectance spectrophotometer (UV–vis DRS) was used to study the optical absorption properties of the HfO_xN_y films. The optical absorbance decreased significantly with the increasing oxygen flow rate. Then the absorbance (A) of samples are calculated as

$$A = -\lg(R), \tag{1}$$

where R is the measured reflectance. Figure 6 shows that all films exhibit an absorption tail near 230 nm and no absorption in the visible region. By applying the following Tauc model and the Davis and Mott model, we obtained the optical band gap (E_g) of the films from the absorption edge[22]

$$\alpha h\nu = D(h\nu - E_g)^n, \tag{2}$$

where α is absorption coefficient, $h\nu$ is the photon energy, D is a constant, and E_g is the optical band gap. Here, the value was calculated using the absorbance instead of the absorption coefficient without obvious effect on the band gap value. We obtained the E_g value from extrapolating the linear part to the zero absorption coefficients. As shown in inset of Fig. 6, the band gap of the films decreases from 5.55 eV to 5.19 eV with increasing oxygen flow rate from 1 to 5 sccm. One possible reason is that the oxygen incorporation will lead to the deterioration of crystalline structure. Combining those material properties, HfO_xN_y film deposited with 1 sccm oxygen is chose for device fabrication.

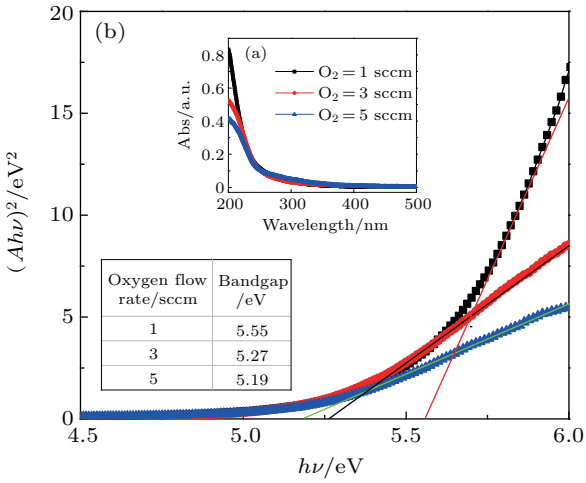


Fig. 6. (color online) The UV–vis spectra of HfO_xN_y films deposited using different oxygen flow rates.

Figure 7 shows the output and gate leakage characteristics of the devices with and without HfO_xN_y dielectric (gate length is 100 μm and gate width is 200 μm). The gate voltage swept from −10 to 1 V with a step of 1 V. All of the devices operate well with the saturation current exhibiting a negative conductance at large drain voltage due to the self-heating and the decreased electron mobility (Fig. 7(a)). The maximum drain current density of MOS HFETs is larger than that of TiN-gated one because of the negative shift of V_{th}. As shown in Fig. 8(a), V_{th} for the Schottky contact, HfO_2, and HfO_xN_y MOS HFETs

are approximately −3.0, −5.0, and −7.0 V, respectively. The corresponding gate current–voltage (I_g–V_g) characteristics of the square-type device also shows that the TiN gated HFETs has a reverse leakage current of about 10^{-6} A (Fig. 7(b)). Then the gate leakage current decreases nearly four orders of magnitude in reverse bias and approximately five to six orders of magnitude in forward by introducing the HfO_2 and HfO_xN_y dielectric. Furthermore, the HfO_xN_y MOS HFETs has much lower forward current compared with the HfO_2 MOS HFETs, which suggested that the HfO_xN_y film is more suitable for the gate dielectric material. However, the transconductance (Gm) of the MOS HFETs is slightly smaller than the Schottky-gated device, owing to the increase of distance between the gate electrode and channel (Fig. 8(b)). The permittivities of the oxide estimated from the capacitance–voltage curves on FATFETs are approximately 12.1 and 10.5 for HfO_xN_y and HfO_2, respectively. Those values are relatively smaller than the theoretical value. The possible reasons are that the crystalline quality is not so good for the sputtered oxide and the real oxide thickness maybe thicker than the nominal one. The interface state information is obtained from the subthreshold swing (SS) value of the device. As calculated from transfer characteristics, the SS values of the HfO_xN_y MOS HFET and TiN HFET are around 161.2 and 100 mV/decade, respectively. The corresponding capacitance of the MOS HFET and HFET are approximately 46.9 pF and 98.6 pF, respectively. Therefore, the interface density (D_{it}) of MOS HFET is approximately 2.87×10^{12} $cm^{-2} \cdot eV^{-1}$.

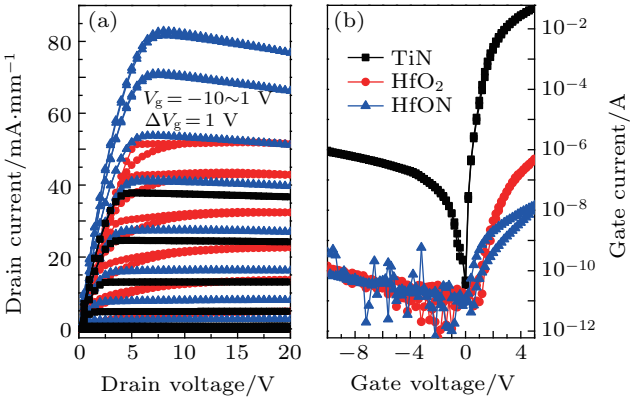


Fig. 7. (color online) (a) The output and (b) gate leakage characteristics of TiN-gated HFETs and MOS HFETs.

To evaluate the thermal stability of the HfO_xN_y and HfO_2 MOS HFETs, we measured the *I*–*V* characteristics of the devices after post deposition annealing at different temperatures (Fig. 9). Figure 9(a) shows a typical output characterization of the HfO_xN_y devices before and after annealed at different temperatures. The device operates well and the output current is comparable with that of the non-annealed one. Figure 9(b) shows the corresponding I_g–V_g characteristics at different annealing temperatures. The forward leakage increases gradually with the increasing annealing temperature from 400 to 900 °C, while the reverse leakage is nearly 10^{-9} A and increases obviously only at 900 °C, which illustrates that HfO_xN_y dielectric has a very good thermal stability. Further increasing the annealing temperature to 1000 °C, the pinch-off characteristic of the device deteriorates with a large leakage current. As a comparison, the output characterization of HfO_2 MOS HFETs device after annealing at 600 °C presents obvious leakage current, as shown in Fig. 10. The leakage current of HfO_2 MOS HFETs deteriorates seriously after annealing at 400 °C (Fig. 10(b)), which is a little higher than that of the HfO_xN_y-gated MOS HFETs at an annealing temperature of 800 °C. A possible reason is that the crystallization temperature of HfO_xN_y film is enhanced from approximately 500 °C (HfO_2) to approximately 900 °C, resulting in a better thermal stability.[13,17] As shown in the UV spectrum, the relatively smaller bandgap of HfO_xN_y should cause the decrease of ΔE_V. However, the leakage current and the thermal stability of the HfO_xN_y are better than the HfO_2. Therefore, the band structure may not determine the high temperature stability. Generally, it demonstrates that adding nitrogen results in the reduction of the mobility of Hf and O atoms and the

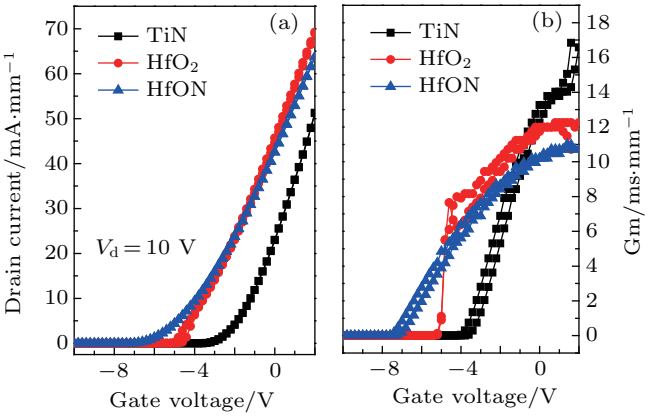


Fig. 8. (color online) The transfer characteristics of the TiN-gated HFETs and MOS HFETs devices.

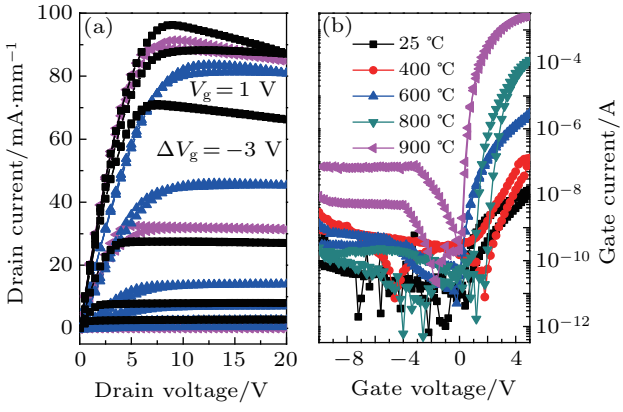


Fig. 9. (color online) (a) The output characteristic of the HfO_xN_y MOS HFETs before and after annealing, and (b) the gate leakage annealed at different temperatures.

maintaining of amorphous structure. Besides, the Hf–N bonding is effective in blocking the oxygen diffusion. Therefore, the HfO_xN_y is believed to increase the nucleation temperature and consequently the crystalline temperature, resulting in an improved thermal stability.[23]

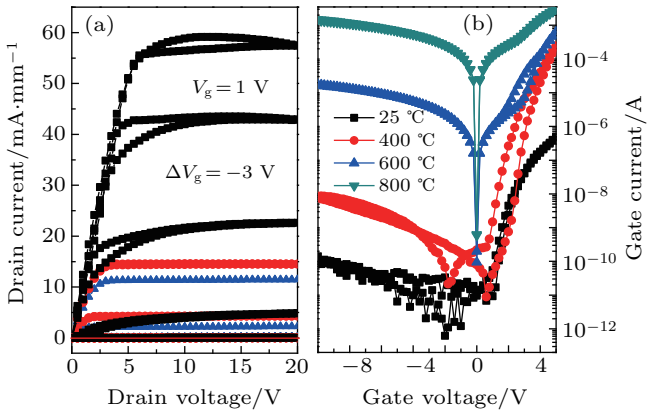


Fig. 10. (color online) (a) The output characteristic of the HfO_2 MOS HFETs before and after annealing, and (b) the gate leakage annealed at different temperatures.

4. Conclusion

We fabricated TiN/HfO_xN_y/AlGaN/GaN MOS HFETs with different oxygen flow rates in the reactive sputtering ambient. The composition of films changed from HfN to HfO_2 domination with the increasing oxygen flow rate and HfO_xN_y formed at a medium oxygen flow rate. Compared with HfO_2 MOS HFETs, the introduction of the HfO_xN_y dielectric results in a negative shifting threshold voltage and a lower leakage current. After post deposition annealing at different temperatures, the devices using HfO_xN_y dielectric show good thermal stability at 900 °C, while obvious degradation are observed for the HfO_2 MOS HFETs at 600 °C. A possible mechanism is that the existence of Hf–N bond in bulk dielectric and N at the dielectric/GaN interface can help to improve the thermal stability.

References

[1] Iwakami S, Yanagihara M, Machida O, Chino E, Kaneko N, Goto H and Ohtsuka K 2004 *Jpn. J. Appl. Phys.* **43** L831
[2] Sang D, Li H and Wang Q 2016 *Nanotechnology* **27** 072501
[3] Zhang J, Wang L, Li L, Wang Q, Jiang Y, Zhu H and Ao J P 2016 *Chin. Phys. B* **25** 087308
[4] Li L, Zhang J, Liu Y and Ao J P 2016 *Chin. Phys. B* **25** 038503
[5] Zhang J, Wang L, Wang Q, Jiang Y, Li L, Zhu H and Ao J P 2016 *Semicond. Sci. Tech.* **31** 035015
[6] Wang L, Zhang J, Li L, Maeda Y and Ao J P 2017 *Chin. Phys. B* **26** 037201
[7] Zhang H and Solanki R 2001 *J. Electrochem. Soc.* **148** F63
[8] Houssa M, Pantisano L, Ragnarsson L A, Degraeve R, Schram T, Pourtois G, De Gendt S, Groeseneken G and Heyns M M 2006 *Mater. Sci. Eng. R-Rep.* **51** 37
[9] Wang G M, Moses D, Heeger A J, Zhang H M, Narasimhan M and Demaray R E 2004 *J. Appl. Phys.* **95** 316
[10] Neumayer D A and Cartier E 2001 *J. Appl. Phys.* **90** 1801
[11] He G, Gao J, Chen H, Cui J, Sun Z and Chen X 2014 *ACS Appl. Mater. Inter* **6** 22013
[12] Zhang J W, He G, Zhou L, Chen H S, Chen X S, Chen X F, Deng B, Lv J G and Sun Z Q 2014 *J. Alloy. Compd.* **611** 253
[13] Kim H, McIntyre P C and Saraswat K C 2003 *Appl. Phys. Lett.* **82** 106
[14] Willk G D, Wallace R M and Anthony J M 2001 *J. Appl. Phys.* **89** 5243
[15] Cheng C L, Liao K S C and Wang T K 2006 *Solid-State Electron.* **50** 103
[16] He G, Fang Q and Zhang L D 2006 *Mater. Sci. Semicon. Proc.* **9** 870
[17] Choi C H, Jeon T S, Clark R and Kwong D L 2003 *IEEE Electr. Device Lett.* **24** 215
[18] Park J H, Hyun J S, Kang B C and Boo J H 2007 *Surf. Coat. Technol.* **201** 5336
[19] Kang C S, Cho H J, Onishi K, Nieh R, Choi R, Gopalan S, Krishnan S, Han J H and Lee J C 2002 *Appl. Phys. Lett.* **81** 2593
[20] Wang W, Nabatame T and Shimogaki Y 2005 *Surf. Sci.* **588** 108
[21] Feng L P, Li N, Tian H and Liu Z T 2014 *J. Mater. Sci.* **49** 1875
[22] Tan S T, Chen B J, Sun X W, Fan W J, Kwok H S, Zhang X H and Chua S J 2005 *J. Appl. Phys.* **98** 013505
[23] He G, Chen X S and Sun Z Q 2013 *Surf. Sci. Rep.* **68** 68